aerospace

MDPI

Article

Towards Optimal Wing Design for Novel Airframe and Propulsion Opportunities

Nicolas F. M. Wahler * and Ali Elham

Department of Aeronautics and Astronautics, University of Southampton, Burgess Road, Southampton SO16 7QF, UK; a.elham@soton.ac.uk

* Correspondence: n.wahler@soton.ac.uk

Abstract: Strict sustainability objectives have been established for the upcoming generation of aircraft. A promising innovative airframe concept is the ultra-high-aspect-ratio Strut-Braced-Wing Aircraft (SBWA). Hydrogen-powered concepts are strong candidates for sustainable propulsion. The study investigates the influence of Liquid Hydrogen (LH2) propulsion on the optimal wing geometry of medium-range SBWA for minimum-cost and minimum-emission objectives. Multiobjective optimizations are performed in two optimization frameworks of differing fidelity for both kerosene- and LH2-propelled SBWA concepts. Furthermore, a range of Pareto-optimal designs show the changes in the optimized planform for variable weighting of the two objectives. The results show that the differences in the optimal wing geometry between the kerosene- and LH2-powered results for each respective objective function are small. For both aircraft, the minimum-emission objective optimizes for lower fuel burns and hence lower emissions, albeit at an increase in wing structural mass. The minimum-cost objective balances the reductions in structural and fuel masses, resulting in a lighter design at lower aspect ratios. Other wing-shape parameters only have minor contributions. Although the wing aspect ratios for both objectives differ by ca. 50%, the actual changes are only 2.5% in fuel and 1.5% in Direct Operating Cost (DOC). Due to a larger set of design variables used in the higher-fidelity optimizations, further parasite and wave drag reduction opportunities result in increased optimal aspect ratios.

Keywords: strut-braced wing; hydrogen; ultra-high-aspect-ratio wing; aerostructural optimization; aircraft design

Academic Editor: Xiaojun Wang

Received: 4 April 2025
Revised: 1 May 2025
Accepted: 20 May 2025
Published: 23 May 2025

Citation: Wahler, N.F.M.; Elham, A. Towards Optimal Wing Design for Novel Airframe and Propulsion Opportunities. *Aerospace* **2025**, *12*, 459. https://doi.org/10.3390/aerospace12060459

1. Introduction

To promote greater sustainability in aviation, the European Commission [1] and NASA [2] have established rigorous sustainability objectives for the upcoming generation of aircraft. With the current aircraft and propulsion technologies approaching their performance limits, achieving these objectives necessitates innovative concepts in both airframe and propulsion designs. One potential airframe innovation is the Ultra-High-Aspect-Ratio Wing (UHARW) [3]. From a purely aerodynamic perspective, for a specified wing area, a higher aspect ratio and thus increased wing span can reduce induced drag, thereby enhancing fuel efficiency. However, the aerodynamic load further away from the wing root also increases the wing's bending moment, which in turn increases the structural mass of the wing, thereby limiting the overall advantages. In conventional medium-range aircraft, the mission fuel mass tends to rise exponentially when the wing aspect ratio exceeds 16 [4]. To mitigate this issue, incorporating a strut in the wing design can decrease the bending

moment by up to 50% [5]. Additionally, utilizing advanced composite materials can further reduce wing weight and provide benefits through aeroelastic tailoring [6]. Incorporating a strut to alleviate bending moments enables a smaller wing structure, with reduced wing thickness and chord length. This reduces transonic wave drag and spanwise crossflow disturbances [7]. This wave drag reduction enables less wing sweep on a design, hence enabling larger areas of laminar flow along the wing [8]. For these reasons, recent studies in UHARWs have focused on the Strut-Braced-Wing Aircraft (SBWA) configuration for transonic mid-range aircraft [5,9,10]. Design studies for short- and long-range designs have also shown benefits over the current designs [11].

In terms of propulsion, hydrogen-based concepts are active contenders for achieving more sustainable aviation, particularly when combined with SBWA to enhance the overall advantages. Since hydrogen combustion with oxygen does not produce CO_2, it will reduce the climate impact compared to kerosene alternatives [12]. Although hydrogen has a higher gravimetric energy density than kerosene, its volumetric energy density is significantly lower. Consequently, while the overall mass of the fuel decreases, the additional storage tanks require a larger airframe. Cryogenic storage improves density, but it also necessitates additional systems and insulation to maintain low temperatures [13]. Designing aircraft with fuel tanks in the fuselage increases the overall wing weight as potential bending moment relief due to wing-based tanks is absent, requiring structural reinforcements for high load factors. Previous studies indicate that the dry wing of Liquid Hydrogen (LH2) aircraft is typically expected to be 7–10% heavier than that of conventional kerosene-fueled aircraft [14,15].

Studies regarding the wing-shape optimization of SBWA have resulted in optimal wing aspect ratios in the range of 14.65 to 20.5 for minimum total fuel objectives [6,8,16–18]. The conventional tube-and-wing concepts used for comparisons in these studies have reached optimal aspect ratios of 11.3 to 12. A comparison for a minimum Maximum Take-Off Mass (MTOM) optimization has resulted in a much lower optimal aspect ratio of 11.8 for the SBWA concept [18]. While this is still marginally larger than the 10.2 of the conventional design used for comparison, it shows that the benefits of the SBWA concept pertain to aerodynamic efficiency and fuel-saving potential, albeit at the risk of a heavier (and more expensive to operate) airframe.

Due to these differences in the wing structure (dry vs. wet wings) and fuselage length between kerosene- and LH2-powered SBWA concepts, as well as the inherent difference in the used fuel type, it is necessary to investigate the effects of LH2 on the optimal wing geometry for an SBWA design.

As such, the objective of this paper is to investigate the effects of LH2 fuel on the optimal wing design for SBWA. Multiobjective optimizations are performed on both kerosene and LH2 concepts, optimizing for trade-offs between minimum emissions and minimum cost. The optimizations are performed in two frameworks of differing fidelity. A lower-fidelity conceptual-level analysis is used to investigate the Pareto-optimal solutions for both concepts. In a second step, the extremes are analyzed in a higher-fidelity aerostructural optimization to investigate the possibility of further performance gains through more detailed wing-shape optimization.

2. Methodology

The study compares wing planform geometries of LH2- and conventional kerosene-based UHARW SBWA optimized for objective functions of minimum Direct Operating Cost (DOC) and minimum fuel burn. Furthermore, Pareto fronts for multiobjective optimizations between minimum DOC and minimum fuel burn at different weight factors are presented for both aircraft.

Optimizations are performed in two frameworks of differing fidelity. The main optimizations are performed using a conceptual analysis tool. In a second step, a higher-fidelity method is used to compare selected points.

2.1. Analysis Methods

2.1.1. Conceptual Analysis Framework

Optimizations have been performed with the open-source Stanford University Aerospace Vehicle Environment (SUAVE) code [19]. The original SUAVE code is modified to integrate hydrogen-powered propulsion systems, hydrogen tank sizing and mass estimations [14,20], SBWA and UHARW geometries and weight estimations [11], along with models for emission and cost analysis [14,21], as further detailed in this section. SUAVE analyzes the performance of the aircraft design throughout a complete mission simulation. It is utilized to optimize the aircraft design for a coherent configuration capable of executing the designated mission, which includes all relevant mission segments. The system iteratively accounts for mass convergence and resizes the aircraft as necessary. Once the aircraft has converged for the mission, a final verification is conducted to ensure that all initial Top-Level Requirements (TLRs) and design specifications remain met before presenting the final design. If any requirements are not satisfied, the sizing process is repeated until all criteria are met.

The mission analysis module requires inputs such as the aircraft geometry, an initial estimation of the MTOM, and details of the flight mission. The main mission is divided into three climb segments, a cruise segment, and five descent segments. The reserve mission consists of two climb segments, a diversion cruise, a hold, and two descent segments. In the vehicle setup, the engine is sized based on the Thrust-to-Weight Ratio (T/W), determined from a constraint diagram. For each segment of the mission, SUAVE employs a root-finding algorithm to solve for a balance of forces, using angle of attack and thrust lever position as variables. The outcomes are utilized to estimate engine thrust and fuel flow for each mission segment. The FLOPS weight estimation approach [22] is applied to calculate the masses of the aircraft components. This weight breakdown, along with the total fuel for the mission, is used to derive an MTOM value. This value serves as an iterated parameter to assess whether the aircraft design has converged or if the wing and propulsion systems need resizing based on the T/W and Wing Loading Ratio (W/S) values from the constraint diagram.

The basic version of SUAVE does not incorporate analysis modules for SBWA designs. For the study of SBWA, a Class II wing weight estimation method has been integrated into the mass module, which includes mass terms for struts [23]. This method relies on a physics-based estimation tool for wing weight, accounting for aileron efficiency and aeroelastic effects.

The reduction in chord along the wing allows larger areas of laminar flow along the wing. Combined with natural laminar flow airfoils, significant drag reductions can be achieved with this concept. To account for both features, a laminar flow of 50% chord is assumed for all SBWA concepts in SUAVE [15].

The strut serves as a structural component that does not contribute to the aircraft's lift while in cruise. Structurally, it is designed in a spindle shape, with the chord sized through buckling requirements. It is attached to the fuselage and the primary wing spar using a symmetric airfoil featuring an 18% maximum thickness-to-chord ratio [23].

The basic SUAVE engine model employs a physics-based cycle analysis methodology [24]. The hydrogen network model includes corrections to the basic turbine performance cycle, as well as sizing and mass estimations for the fuel tanks based on stress limits [20]. The designs use Ultra-High-Bypass-Ratio (UHBR) engines.

The mass estimations for the additional components of the fuel system linked to the hydrogen network are divided into two sections [14]. The fuel tank is sized actively through a structural and thermodynamic assessment [25]. The auxiliary components are sized using constant values [13].

The necessary size of the fuel tank is established iteratively based on the mission fuel requirements, boil-off losses resulting from the tank's thermodynamic properties, and the fuselage shape. This thermodynamic model calculates internal pressure fluctuations and heat transfer within the tank at each time increment during the mission [26].

The final mass of the tank is determined by analyzing the hoop and dome stresses of the resulting structure [25]. By utilizing the limit load factor and the maximum pressure differential between the hydrogen and the ambient environment, the required thicknesses of the structural walls are calculated, with aluminum assumed as the tank material in this design.

2.1.2. Aerostructural Analysis Framework

SUAVE as a conceptual design framework is well suited for rapid analysis and geometry optimization. However, the linear aerodynamic solvers used to compute lift and drag are limited in their fidelity. As such, a second set of optimizations are performed with a higher-fidelity simulation tool, which can account for more wing and airfoil shape parameters than the SUAVE analysis.

The core of this aerostructural optimization framework is FEMWET, a coupled adjoint aerostructural wing optimization tool [27]. This tool integrates a Quasi-Three-Dimensional (Q3D) aerodynamic solver with a nonlinear finite beam element structural solver. The Q3D solver combines a Vortex Lattice Method (VLM) code with MSES, a two-dimensional compressible airfoil analysis tool. The wing lift, spanwise lift distribution, and induced drag are computed using the VLM part, including a Prandtl–Glauert correction for compressibility effects. MSES is used to improve the fidelity of the aerodynamic analysis and predict the laminar–turbulent transition. Using the incidence angle (α_i) as additional variable, the sectional lift coefficients of the VLM and MSES are matched, accounting for wing sweep. Viscous, pressure, and wave drag of the wing are then found by integrating the two-dimensional results along the wing span.

FEMWET was modified for the analysis of SBWA by including a geometrically nonlinear structure model [28,29]. These modifications allow FEMWET to account for large displacements and rotations inherent in lightweight, flexible SBWA designs.

The wing shape is discretized into a number of sequential wing box sections, as shown in Figure 1. Each wing box section is composed of four panels (upper, lower, front, and rear) with individually associated panel thicknesses.

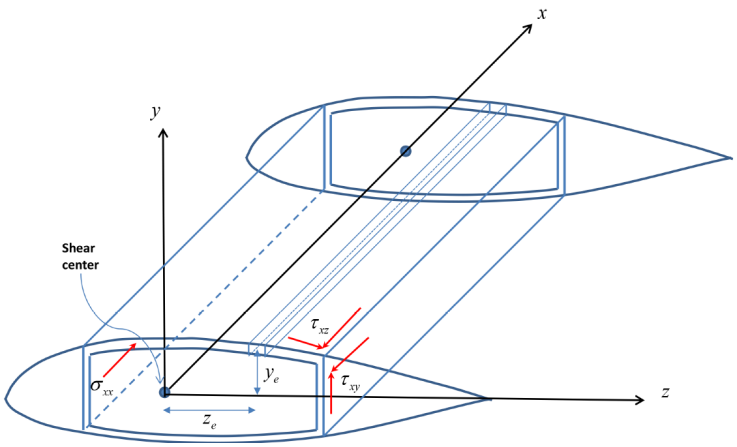

Figure 1. Wing box segment and panel positions [30].

The coupled aerostructural system as shown in Equation (1) is defined by four governing equations: those of the VLM, Finite Element Method (FEM), level flight conditions, and the Q3D method. The first two equations represent the governing equations of the VLM (A) and FEM (S). The third equation (W) ensures that lift and weight forces are equal at the design load factor. The last equation (C) affirms that the two-dimensional sectional lift from MSES is equal to the lift computed by the VLM. The Newton method solves Equation (2) iteratively using the state variables of circulation (Γ), velocity (U), angle of attack (α), and incidence angle (α_i).

$$\begin{bmatrix} A(X,\Gamma,U,\alpha) \\ S(X,\Gamma,U) \\ W(X,\Gamma) \\ C(X,\Gamma,U,\alpha,\alpha_i) \end{bmatrix} = 0 \tag{1}$$

The state variables in the system are found iteratively using a Newton method to solve the governing equations shown in Equation (2).

$$\begin{bmatrix} \frac{\partial A}{\partial \Gamma} & \frac{\partial A}{\partial U} & \frac{\partial A}{\partial \alpha} & \frac{\partial A}{\partial \alpha_i} \\ \frac{\partial S}{\partial \Gamma} & \frac{\partial S}{\partial U} & \frac{\partial S}{\partial \alpha} & \frac{\partial S}{\partial \alpha_i} \\ \frac{\partial W}{\partial \Gamma} & \frac{\partial W}{\partial U} & \frac{\partial W}{\partial \alpha} & \frac{\partial W}{\partial \alpha_i} \\ \frac{\partial C}{\partial \Gamma} & \frac{\partial C}{\partial U} & \frac{\partial C}{\partial \alpha} & \frac{\partial C}{\partial \alpha_i} \end{bmatrix} \begin{bmatrix} \Delta\Gamma \\ \Delta U \\ \Delta\alpha \\ \Delta\alpha_i \end{bmatrix} = - \begin{bmatrix} A(X,\Gamma,U,\alpha) \\ S(X,\Gamma,U) \\ W(X,\Gamma) \\ C(X,\Gamma,U,\alpha,\alpha_i) \end{bmatrix} \tag{2}$$

The aerostructural coupling includes a transfer of aerodynamic loads from the aerodynamic VLM mesh to the structural FEM mesh, and the transfer of displacements from the FEM to the VLM solver. The six-degree-of-freedom deformation movements of every node in the FEM are applied to the VLM mesh at every Newton iteration. The aerodynamic forces are applied to the deformed FEM mesh. Meshing for both methods is conducted such that the nodes coincide; thus, no interpolation between the meshes is necessary. Figure 2 shows an example of the VLM and FEM meshes for the SBWA.

In the Q3D method the interference drag between wing and strut (and also wing and fuselage) cannot be modeled, so an interference factor of 10% [31] is applied.

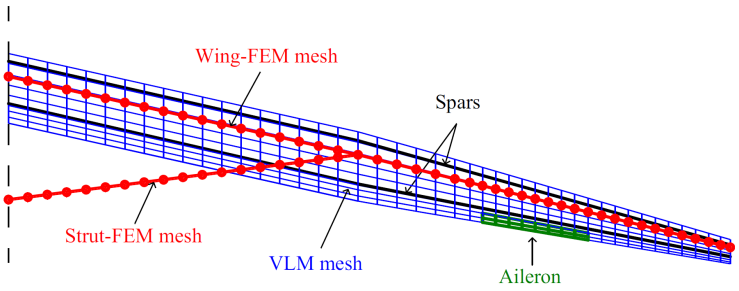

Figure 2. Example of aerodynamic and structural meshes for an SBWA.

Past studies have indicated that the aileron effectiveness requirements act as active limitations in the structural design of the SBWA wing [15,29]. It has been demonstrated that the structural weight of the wing increases quadratically based on the effectiveness requirements of the aileron [32]. Consequently, a constraint is implemented to ensure that the roll performance criteria of the aircraft are met. The constraint is implemented by simulating the achievable rolling moment at full aileron deflection, with the flexible and deformed wing in the VLM code. The derivative of change in lift due to aileron deflection is computed and compared against a lower bound of the parameter. This lower bound was pre-determined [32] to ensure that a sufficient minimum rolling moment is created, in accordance with handling quality regulations. If an insufficient moment is created, then the wing rigidity needs to be increased, at the expense of additional structural mass. Further

information regarding the aileron design for this SBWA and the importance of including roll moments in an aerostructural optimization for SBWA can be found in [32].

Table 1 shows the different limiting load cases that were considered for structural sizing within the aeroelastic optimizations. These four load cases are each characterized by different weights, altitude, Mach numbers, and load factors. The specific flight conditions and masses are based on an analysis of critical load cases within the flight envelope of the aircraft, similar to [33].

Table 1. Load cases of the SBWA.

Load Case	Type	Weight	Altitude [m]	Mach	Load Condition [g]
1	Pull-up	MTOM	7500	0.78	2.5
2	Push-down	MTOM	7500	0.78	−1
3	Roll	W_{design}	4000	0.75	1
4	Cruise	W_{design}	10,058	0.735	1

To determine the aircraft fuel burn at the nominal mission in FEMWET, the Breguet range equation and the fuel fraction estimation method are used in the mission analysis section. The Breguet range equation shown in Equation (3) is used to estimate the necessary fuel mass for all fuel-intensive flight phases of the nominal mission. For all other flight phases, a cumulative fuel fraction (M_{ff}) is computed as a fraction of the total mass [34]. Total fuel is then found following Equation (4). The relevant performance parameters of flight speed (V), thrust-specific fuel consumption (SFC), as well as fuel fractions are obtained from the SUAVE models of the reference aircraft.

$$R = \frac{V}{SFC} \cdot \left(\frac{L}{D}\right) \cdot log\frac{W_{initial}}{W_{final}} \tag{3}$$

$$M_f = \left(1 - M_{ff}\right) \cdot MTOM \tag{4}$$

As FEMWET only estimates the aerodynamics and mass properties of the main wing and strut system, fixed values are assumed for the remaining aircraft structure drag and mass. These are computed by subtracting the FEMWET equivalent wing and strut drag and mass values from the original full aircraft parameters. The remainders are then assumed constant throughout the optimization. Within an optimization step, the current wing geometry is evaluated by FEMWET, and the current wing/strut drag and mass values are added to the constants to compute aircraft total properties.

The individual modules as well as the complete tool have been extensively verified in previous studies. The aerodynamic solver has been validated against the higher-fidelity MATRICS-V tool [27]. The structural mass estimation has been validated against an A320 main wing and horizontal tail, showing errors of less than 1% [35]. The nonlinear structural analysis models have been verified in [29,36].

2.2. Modifications of Both Frameworks

Both frameworks require additional modules to evaluate emissions and operating costs for the designs throughout the optimizations. The models were initially implemented in the SUAVE tool [15]. In a second step, modified versions were implemented into FEMWET, adapted for FEMWET input and output requirements.

2.2.1. Cost Estimation

The optimization framework includes a module to estimate DOC and production costs [14,21]. The overall DOC represents the total of energy, maintenance, capital, crew,

and fee elements [37]. A maintenance gain factor is included to reflect the impact of advanced aircraft technologies. This adjustment factor is assumed to represent the added maintenance complexities associated with SBWA and the hydrogen infrastructure [15].

The original cost model for pricing airframes is derived from Roskam [38], with an additional consideration for capital costs to incorporate the expenses related to the LH2 tank [39].

2.2.2. Emission Estimation

The second required module calculates the total mission emissions of the aircraft. The emission model that has been implemented [14,21] is derived from the methods outlined in [12,40] for determining the Sustained Global Temperature Potential (SGTP).

To ensure comparability, the final emissions are presented as equivalent CO_2 emissions in Equation (5), incorporating actual CO_2, NO_x, contrails, cirrus clouds, and production emissions.

$$\begin{aligned} m_{CO_2,eq} = (&k_0 EI_{CO_2} f_{km} + k_1 k_2 EI_{NO_x} f_{km} CH_{mid,NO_x} \\ &+ k_3 k_4 CF_{mid,AIC}) \Delta R_{km} + m_{CO_2,eq,production} \end{aligned} \tag{5}$$

The Emission Index (EI) for CO_2 remains constant at 3.16, whereas, for NO_x, it varies based on fuel type and flight conditions [41]. f_{km} denotes the fuel flow rate, and ΔR_{km} represents the incremental flight distance. Emissions for Aviation-Induced Cloudiness (AIC), which include the effects of contrails and cirrus, depend solely on altitude and range in this model. The Correction Factors (CFs) for the emission species change with the altitude of the aircraft [42]. To reflect variations during the mission, the emission model is integrated into the SUAVE mission analysis for computing localized emissions throughout the mission. Ultimately, the emissions are adjusted to match the fuel type in Equation (5) using constants $k_1 - k_4$. The impacts of fuel production are considered in the kerosene model as accounting for 22% of total flight emissions [21]. In the case of the LH2 model, emissions are contingent on the hydrogen production process. The production emissions associated with green hydrogen discussed in [43] are utilized in this study.

The SUAVE simulation results account for all in-flight emissions according to the actual flight conditions along all segments of the flight mission according to this model. The FEMWET results, due to the simpler mission simulation module using the Breguet range equation, only account for the emissions in cruise phases.

2.3. Optimization Formulations

2.3.1. Conceptual Analysis Optimization Problem

The SUAVE-based optimization is using the native optimization functionalities in SUAVE. This is a wrapper for the gradient-based Sequential Least Squares Quadratic Programming (SLSQP) optimization function in SciPy. The actual SUAVE analysis is treated as a black-box function. Gradients are computed numerically purely based on the black-box results. Due to the simpler nature of the analyses, the four primary wing planform parameters aspect ratio (AR), taper ratio (λ), quarter-chord wing sweep (Λ), and wing-thickness-to-chord ratio (t/c) are used for the optimization. The optimization formulation is shown in Equation (6). The objective function of this multiobjective optimization problem concerns a trade-off between the total operating costs and total emissions of the flight mission. The weight factor (k) is variable.

$$\begin{aligned} min \quad & k\frac{DOC(X)}{DOC_{baseline}} + (1-k)\frac{Emission(X)}{Emission_{baseline}} \\ w.r.t \quad & X = [AR, \lambda, \Lambda, (t/c)] \\ s.t. \quad & X_{lower} \leq X \leq X_{upper} \end{aligned} \tag{6}$$

Further constraints are not necessary in this case as the internal iteration routine described in the earlier subsection ascertains that the aircraft wing, propulsion system, and LH2 storage (if applicable) are resized to adhere to the original design W/S and T/W parameters.

2.3.2. Aerostructural Analysis Optimization Problem

The aerostructural optimization using FEMWET is using a more complex optimization setup. The full Extended Design Structure Matrix (XDSM) showcasing a Multi-Disciplinary-Feasible (MDF) architecture is presented in Figure 3. Similar to the SUAVE internal optimization routine, the FEMWET core (comprising the VLM, FEM, weight analysis, and Q3D disciplines) is using an internal Multi-Disciplinary Analysis (MDA) to converge the aerodynamic and structural disciplines and their coupling internally for each objective function evaluation. The results are used in the emission and cost analysis disciplines to compute the objective function and all relevant constraints. Consistency variables (subscript *s*) are used in the outer optimization loop to enforce feasible results.

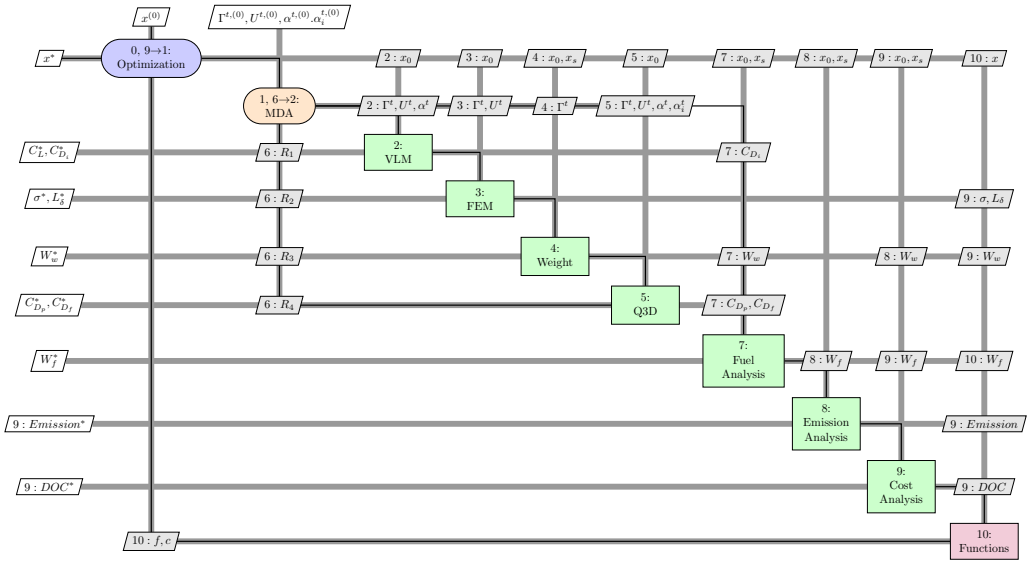

Figure 3. Extended design structure matrix of aerostructural multi-disciplinary design optimization framework.

The new optimization formulation used in this second step shown in Equation (7) is adapted from [29], using the same objective function as the SUAVE-based optimization. The higher fidelity of the wing analysis module allows additional design variables to be considered. The design variables now include the thicknesses ($t_{u_i}, t_{l_i}, t_{fs_i}, t_{rs_i}$) of wing and strut structural elements (upper and lower skins, and front and rear spars), wing and strut airfoil shapes (G, G_{st}), wing planform geometry (P), and two surrogate variables ($M_{FS}, MTOM_S$). The wing structural elements are a sequence of wing box sections (i) along the wing span, with skin and spar thicknesses as shown in Figure 1. The airfoil shapes at the specific spanwise position are parameterized using Chebyshev polynomials, using 10 modes per airfoil surface. The wing planform geometry vector includes not only aspect

ratio, taper ratio, and leading-edge sweep angle but also root chord and two twist angles at the wing kink and tip, respectively. The optimization additionally requires two surrogate variables, fuel weight and MTOM, to avoid additional iterations between performance calculation and aerostructural analysis as shown in Figure 3.

$$\begin{aligned}
min \quad & k\frac{DOC(X)}{DOC_{baseline}} + (1-k)\frac{Emission(X)}{Emission_{baseline}} \\
w.r.t \quad & X = [t_{u_i}, t_{l_i}, t_{fs_i}, t_{rs_i}, G, G_{st}, P, M_{FS}, MTOM_S] \\
s.t. \quad & Failure_k \leq 0 \\
& 1 - \frac{L_\delta}{L_{\delta,min}} \leq 0 \\
& \frac{MTOM/S_w}{MTOM_0/S_{w0}} - 1 \leq 0 \\
& \frac{M_F}{M_{FA}} - 1 \leq 0 \\
& \frac{M_F}{M_{FS}} - 1 = 0 \\
& \frac{MTOM}{MTOM_S} - 1 = 0 \\
& X_{lower} \leq X \leq X_{upper}
\end{aligned} \tag{7}$$

The additional constraints now account for structural properties and deflections. The first set of constraints ensures that the structure satisfies a set of conditions regarding failure under tension or compression as well as Euler and shear buckling in the specified load cases. The failure criteria for tension and compression are equivalent stresses. For buckling predictions, the Engesser method [44] is used. The second constraint ascertains that a minimum required roll moment due to aileron deflection is achieved. The derivative of change in lift due to aileron deflection (L_δ) is computed and compared against a lower bound of the parameter [32]. Two additional constraints are imposed to ensure that the new wing loading and fuel mass are lower or equal to the initial values to keep the performance equal or better than the reference aircraft. The final two constraints state that the actual MTOM and fuel mass need to be equal to their surrogate values to keep the aircraft design physically feasible.

2.4. Reference Aircraft Designs

The baseline aircraft for the optimizations were designed and investigated in a previous study [15]. Sizing and performance estimations were performed using the modified SUAVE code described in the previous sections. More information on the sizing process and aircraft performance estimation for both designs is presented in [15].

Both the conventional and LH2-based design concepts are designed to comply with EASA CS-25 standards [45], featuring TLRs akin to the Airbus A320neo. The primary modification aimed at enhancing the aircraft's energy efficiency was the reduction in the cruise Mach number to M0.735, as suggested by [46]. The TLRs of the designs in this study are detailed in Table 2.

The designs feature an aspect ratio of 25 and incorporate several advanced airframe technologies [11]. Featuring strut-braced wings, the aircraft utilize Natural Laminar Flow (NLF) airfoils, which result in an increase in laminar flow to 50% chord length across the wings. Advancements in materials and structural designs, particularly tow-steering of composites, enable a weight reduction of 20% compared to traditional metal structures.

Table 2. Top-level design requirements for the SBWA.

Parameter		Value
Cruise Mach number		0.735
Max. Mach number		0.82
Passengers		150
Range		3400 nm
Reserves	Contingency fuel	3%
	Diversion range	200 nm
	Holding (1500 ft)	10 min
Cruise altitude		33,000 ft
Service ceiling		38,500 ft
Takeoff field length		<6400 ft (ISA and sea level)
Landing distance		<4500 ft (ISA and sea level)
Approach speed		136 kts true airspeed
Airport (ICAO C)	Wing span	36 m
	Main landing gear span	9 m
Certification regulation		CS-25

The design mission profile for the aircraft is illustrated in Figure 4. Within the framework of SUAVE, the mission is discretized into multiple segments. The aircraft has a main mission range of 3400 nautical miles, plus a 200 nautical mile diversion segment and 10 min of holding fuel. For the main mission, both climb and descent are broken down into three segments each, each characterized by constant speed and constant climb or descent rates. Additionally, a reduced contingency factor of 3% of the trip fuel is considered [11].

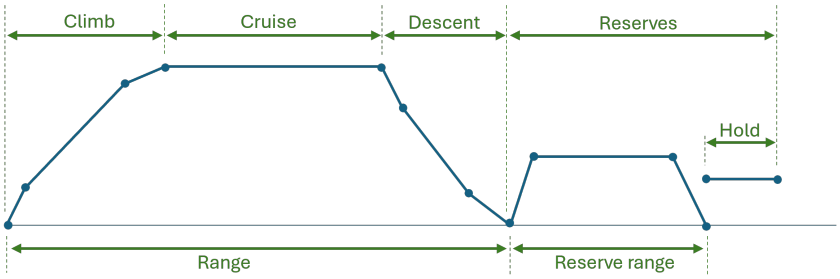

Figure 4. SBWA mission profile.

To visualize these designed concepts, Figure 5 displays the resulting aircraft geometries, generated using OpenVSP 3.37.1.

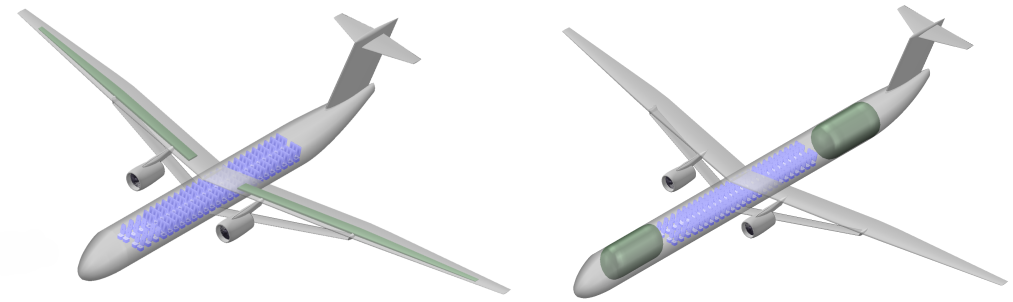

(**a**) Kerosene concept (**b**) LH2 concept

Figure 5. Isometric view of both reference SBWA concepts [15].

Tables 3 and 4 summarize comparisons of the key geometry and mass parameters of the two baseline configurations.

Table 3. Aircraft geometry comparison between kerosene and LH2 SBWA designs.

Parameter	Kerosene	LH2
Wing		
Aspect ratio	25	25
Span	63.08 m	64.44 m
Area	159.14 m^2	166.13 m^2
Taper ratio	0.35	0.35
Quarter-chord sweep	12.5°	12.5°
Root chord	3.02 m	3.08 m
Dihedral	−1.5°	−1.5°
Root, tip, and kink thickness	11.4%	11.4%
Strut		
Aspect ratio	23.03	23.03
Span	31.41 m	32.08 m
Area	42.83 m^2	44.71 m^2
Taper ratio	0.8	0.8
Quarter-chord sweep	9.87°	9.92°
Root chord	1.5 m	1.54 m
Dihedral	7.67°	7.50°
Thickness	18%	18%
Fuselage		
Length	39.0 m	52.4 m
Diameter	4.1 m	4.1 m

Table 4. Aircraft mass comparison between kerosene and LH2 SBWA designs.

Parameter	Kerosene	LH2	Difference	A320neo for Reference [47]
MTOM	67,556 kg	69,678 kg	+3.14 %	79,000 kg
Fuel	13,682 kg	5520 kg	−59.7 %	20,980 kg
Empty	39,654 kg	49,100 kg	+23.8 %	44,300 kg
Propulsion	4611 kg	4873 kg	+5.68%	
Nacelles	532 kg	544 kg	+2.26 %	
Landing gear	2280 kg	2346 kg	+2.89%	
Wing	11,417 kg	11,981 kg	+4.94%	
Horizontal tail	413 kg	400 kg	−3.15%	
Vertical tail	900 kg	772 kg	−14.2%	
Fuselage	7066 kg	9881 kg	+39.8%	
Systems	11,984 kg	12,417 kg	+3.61%	
LH2 tanks	-	5357 kg	-	
Paint	450 kg	528 kg	+17.3%	

3. Results

3.1. Conceptual Optimization Results

The initial values and applicable bounds for the conceptual-level optimization are shown in Table 5. The initial values are taken from the baseline aircraft designs [15], adapted from [11]. These values are based on design choices and handbook values but are not optimized yet. Lower and upper bounds are set to cover the whole expected design space while limiting the results to feasible values given the design mission.

Tables 6 and 7 compare the results for the minimum-emission and minimum-cost optimizations for the kerosene and LH2 concepts, respectively.

The minimum-emission objective functions yield lower fuel burn and hence lower emissions. These optimizations lay a larger focus on the aerodynamic performance of the aircraft. While the increased structural mass incurs a performance penalty, the reduction in wing-induced drag outweighs this penalty.

Table 5. Conceptual-level optimization design variable initial values and bounds.

Design Variable	Initial Value	Lower Bound	Upper Bound
Aspect ratio	25	10	30
Taper ratio	0.35	0.25	0.6
Quarter-chord sweep	12.5°	5°	25°
Thickness-to-chord ratio	0.114	0.05	0.18

The minimum-cost objective function has a more balanced approach to reduce both structural and fuel masses. While fuel burn is a significant part of the total mission cost, many other parameters, such as maintenance, capital, and airway costs, are functions of the aircraft MTOM. As such, reducing the total mass of the aircraft concept will outweigh aerodynamic efficiency when optimizing for minimum cost.

These principles can be seen well in the tables. The minimum-emission objective converges to 50% larger aspect ratios than the minimum-cost function. While increased aspect ratios reduce the wing-induced drag, the higher wingspan leads to increased bending moments at the wing root and hence requires a stronger and heavier wing structure. Larger wing spans also increase the size, drag, and mass of the strut as it is attached at a fixed 50% of the wing semi-span. As such, higher aspect ratios lead to higher aerodynamic efficiency but also higher structural mass, as seen in the wing weight comparisons. Even though the fuel mass is reduced, the overall aircraft is still heavier in MTOM than at a lower aspect ratio.

Table 6. Minimum-emission and minimum-cost optimization results for kerosene SBWA from SUAVE.

Parameter	Reference	Min. Emission	Min. Cost
Aspect ratio	25	15.49	10.80
Taper ratio	0.35	0.30	0.33
Quarter-chord sweep	12.5°	18.12°	12.96°
Thickness-to-chord ratio	0.114	0.064	0.080
Fuel	13,682 kg	12,872 kg	13,215 kg
Cost	EUR 46,277	EUR 43,967	EUR 43,127
Emission	259,830 kg_{CO2eq}	255,918 kg_{CO2eq}	257,561 kg_{CO2eq}
MTOM	67,556 kg	63,636 kg	60,746 kg
Wing weight	11,417 kg	8779 kg	5896 kg

The aspect ratios of the optimized aircraft are much lower than the initial value of 25. For minimum emissions, the results are well within the range of 14.5 to 20 as supported by other literature results regarding SBWA optimizations [6,8,16–18]. Higher-fidelity optimizations (see Section 3.2) show larger aspect ratios, closer to the initial value of 25. The reasons for this difference are discussed in Section 3.2.

Table 7. Minimum-emission and minimum-cost optimization results for LH2 SBWA from SUAVE.

Parameter	Reference	Min. Emission	Min. Cost
Aspect ratio	25	15.58	10.899
Taper ratio	0.35	0.441	0.363
Quarter-chord sweep	12.5°	16.7°	12.97°
Thickness-to-chord ratio	0.114	0.0628	0.0810
Fuel	5520 kg	5222 kg	5389 kg
Cost	EUR 54,377	EUR 51,421	EUR 50,356
Emission	155,716 kg_{CO2eq}	155,555 kg_{CO2eq}	155,637 kg_{CO2eq}
MTOM	69,678 kg	65,481 kg	62,203 kg
Wing weight	11,981 kg	9171 kg	6119 kg

The visual representations overlaying the resulting wing shapes per propulsion concept, as shown in Figures 6 and 7, indicate that all the optimized wings have lower aspect ratios but higher chord lengths than the reference wing. While the wing shapes are slightly different, the optimal aspect ratios per optimization objective are similar for both the kerosene and LH2 results. For the kerosene results, both optimized wings have higher sweep angles but lower taper ratios than the reference. For the LH2 results, the taper ratios are higher, but the sweep angles are lower than for the kerosene results.

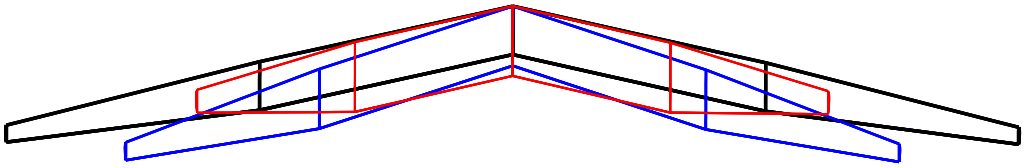

Figure 6. Visualization of the kerosene SBWA wing shapes from the conceptual optimizations for reference (black), minimum-fuel (blue), and minimum-cost (red) designs.

Wing quarter-chord sweep and thickness-to-chord ratios influence the wing drag and mass. Lower sweep and thicker wings reduce the wing structural mass but increase the parasitic and wave drag. As such, a minimum-cost wing has a thicker but less swept wing than for minimum emissions, as shown in the tables.

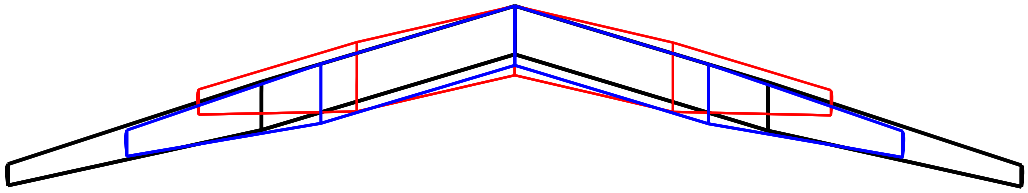

Figure 7. Visualization of the LH2 SBWA wing shapes from the conceptual optimizations for reference (black), minimum-fuel (blue), and minimum-cost (red) designs.

Pareto fronts showing the trade-off between emission and DOC objectives are presented in Figure 8. The figures show the changes in cost and emission of optimal designs for varying k-factors.

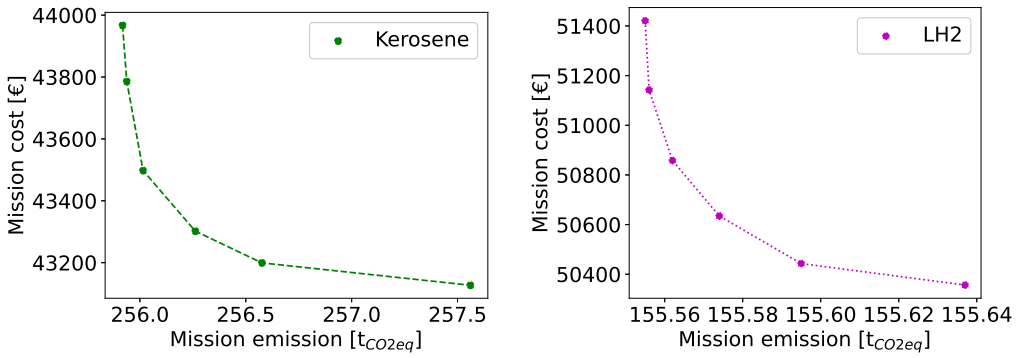

(**a**) Kerosene (**b**) LH2

Figure 8. Resulting cost–emission Pareto fronts for kerosene- and LH2-based SBWA.

Figure 9 shows a comparison of the relative changes in the optimal cost, fuel, and emission results for varying k-factors compared to the respective baseline aircraft. $k = 0$ is equivalent to an emission-only minimization; $k = 1$ equals a cost-only optimization. The intermediate points represent varying weight factors in 20% increments. The results show that, even though at each point the aspect ratios (and thus wing spans) of the designs are

quite different, the actual changes in fuel, emission, and cost are small. The shapes of the respective curves for kerosene and hydrogen are similar, indicating that the fuel type has no significant influence on the optimization behavior. Between the two extremes, changes in fuel of about 2.5% and changes in DOC of about 1.5% can be expected. The total emissions are nearly unchanged by the weight factor. This is partially due to the emission model. It accounts for changes in fuel burn at different altitudes throughout the mission. However, the formation of contrails is treated in a simplified manner. The model does not consider the actual wing-shape geometry for computing the contrail emissions, which comprise the largest individual contributing factor to the total emission values.

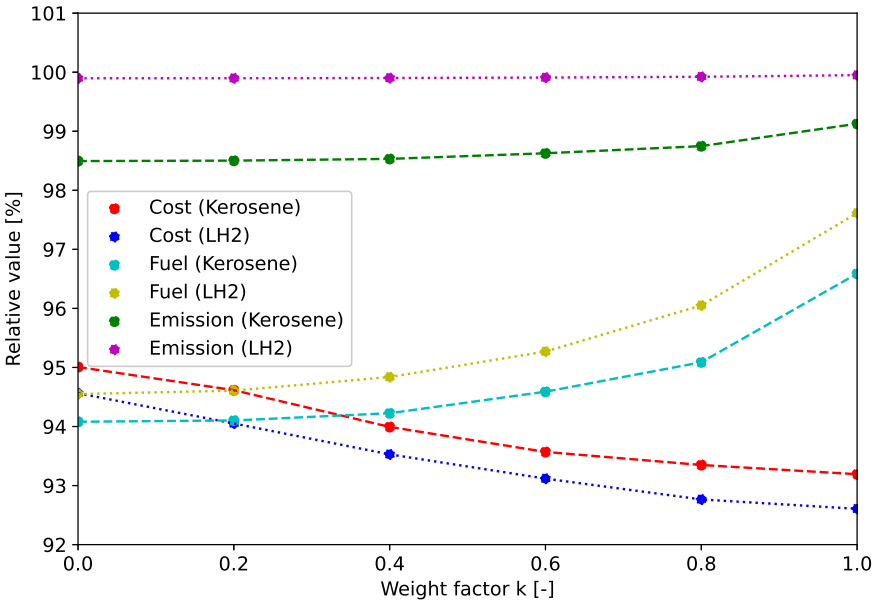

Figure 9. Relative changes in optimized values compared to the reference aircraft of kerosene and LH2 results for varying k-factors.

The changes in the wing geometry parameters for varying k-factors are shown in Figure 10. Comparing the results for the hydrogen and kerosene aircraft at the same objective function shows that both aircraft optimize to similar results for all the k-factors. As discussed earlier, the aspect ratio shows a monotonous decrease from the minimum emissions towards the minimum DOC. It also has the largest change in the four parameters. Furthermore, it shows that the aspect ratio and thickness-to-chord ratio are larger design drivers than the other two parameters as they show less variability in their results. They both show strong trends that are nearly identical for the kerosene and hydrogen concepts. The taper ratio is nearly constant for $k \leq 0.6$ and again for $k > 0.6$, with a small jump in between. The results could indicate that, for the LH2 concept, a higher taper is beneficial; however, the overall difference is small. The quarter-chord sweep also shows only secondary importance. While a slight downward trend is visible for an increasing k-factor, the large variability indicates that the sweep, within these limits, has only a minor influence on the overall optimal designs.

Finally, Figure 11 compares the resulting MTOMs and wing masses. As expected, the emission-optimal results also yield the highest wing and overall masses, while the cost-optimal results yield the lowest masses. The wing masses are up to 25% lower. However, as the wing mass is only a small part of the total, the overall change in MTOM is only 4%.

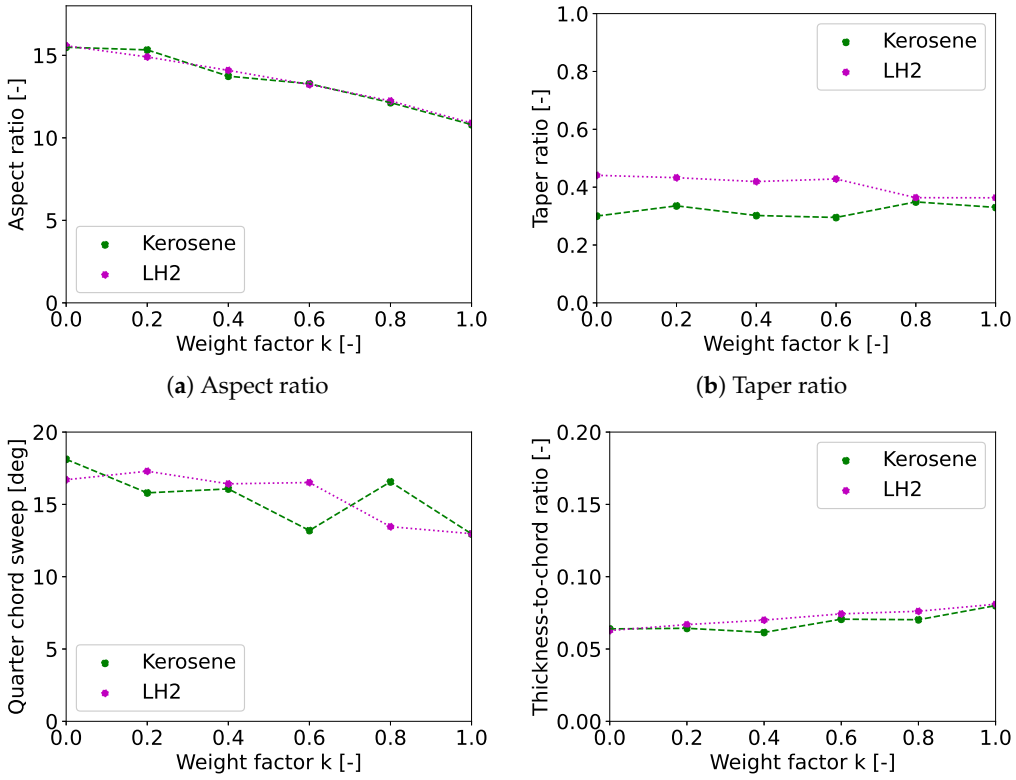

(**a**) Aspect ratio (**b**) Taper ratio

(**c**) Quarter-chord sweep angle (**d**) Thickness-to-chord ratio

Figure 10. Optimized geometry results for kerosene- and LH2-based SBWA for varying k-factors.

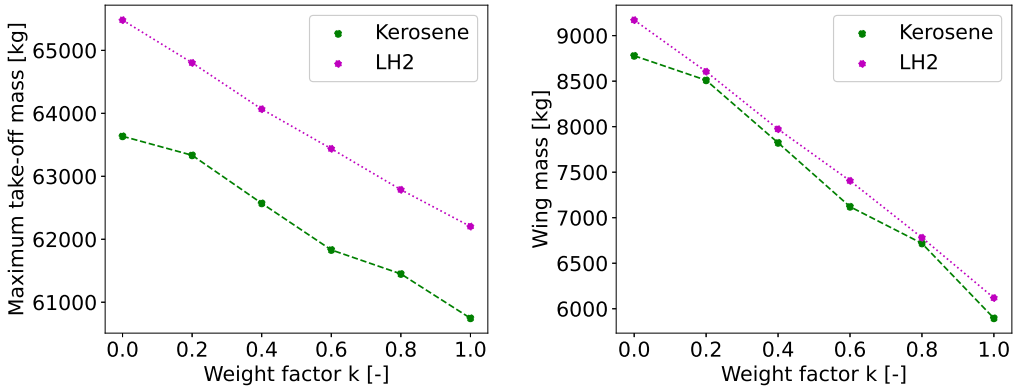

(**a**) MTOM (**b**) Wing mass

Figure 11. Optimized mass results for kerosene- and LH2-based SBWA designs for varying k-factors.

3.2. Aerostructural Optimization Results

The aerostructural optimizations were performed with the FEMWET framework. Tables 8 and 9 showcase the results for minimum emission and cost using the higher-fidelity aerostructural optimizations. The main difference lies in the higher aspect ratios compared to the SUAVE-based optimizations, which are 32 to 59% larger than the respective SUAVE results.

The visual representations of the resulting wing shapes presented in Figures 12 and 13 show that both optimized wings have lower aspect ratios than the reference wing. The minimum-emission wings have similar sweep angles and taper ratios to the reference. Especially, the LH2 minimum-emission wing is very similar to the reference design, showing only small differences in aspect ratio and sweep. The minimum-cost wings compensate

for an even lower aspect ratio with a larger root chord and higher taper ratio while also increasing the wing sweep.

Table 8. Minimum-emission and minimum-cost optimization results for kerosene SBWA from FEMWET.

Parameter	Reference	Min. Emission	Min. Cost
Aspect ratio	25	21	15
Taper ratio	0.35	0.37	0.5
Leading-edge sweep	12.5°	11.63°	17.06°
Fuel	13,682 kg	10,713 kg	11,153 kg
Cost	EUR 46,540	EUR 40,509	EUR 40,455
Emission	270,250 kg_{CO2eq}	251,070 kg_{CO2eq}	253,820 kg_{CO2eq}
MTOM	67,556 kg	58,924 kg	57,960 kg
Wing weight	14,117 kg	8454 kg	7059 kg

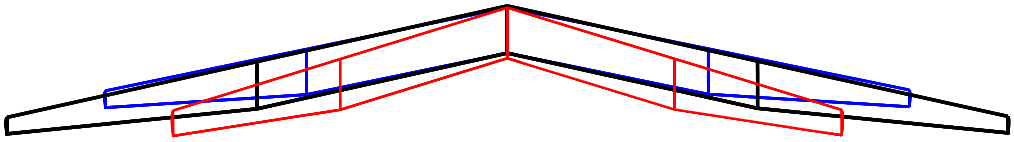

Figure 12. Visualization of the kerosene SBWA wing shapes from the aerostructural optimizations for reference (black), minimum-fuel (blue), and minimum-cost (red) designs.

The main reasons for this change are differences in the aerodynamic solver and the available design parameters. FEMWET's higher-fidelity solver is able to predict friction and wave drag more accurately. Furthermore, the thickness of the strut as well as the airfoil shapes of the wing are additional design variables in the optimization. FEMWET optimized the airfoil shapes to reduce the shock wave formation, hence reducing the wave drag. Strut thickness optimizations led to a thinner strut structure, which reduced the strut drag. The inclusion of strut variables in the optimization is important as the strut has a major contribution to the total wing drag. This was not included in the optimizations with SUAVE as the low-fidelity weight method of SUAVE is not sensitive to the details of the strut geometry. Increasing the aerodynamic efficiency of the strut, as well as the full wing-shape optimization (beyond only optimizing the thickness-to-chord ratio), allowed the optimizer to increase the wing aspect ratios beyond the SUAVE optima, with lower penalties in drag and weight.

Table 9. Minimum-emission and minimum-cost optimization results for LH2 SBWA from FEMWET.

Parameter	Reference	Min. Emission	Min. Cost
Aspect ratio	25	24.81	14.35
Taper ratio	0.35	0.33	0.48
Leading-edge sweep	12.5°	10.82°	13.62°
Fuel	5520 kg	4621 kg	4787 kg
Cost	EUR 54,771	EUR 50,702	EUR 48,924
Emission	152,240 kg_{CO2eq}	151,250 kg_{CO2eq}	151,430 kg_{CO2eq}
MTOM	69,678 kg	65,117 kg	61,535 kg
Wing weight	14,368 kg	11,379 kg	7508 kg

Taper ratios and sweep show similar results to the SUAVE optimizations. Although the sweep seems to indicate an opposite trend (higher sweep for minimum cost), both values are within the margins of the SUAVE multiobjective optimization results, and hence a definite conclusion is not possible with the current data. The taper ratios for the minimum emission results are in agreement with SUAVE; for the minimum cost optimizations the taper ratios are higher.

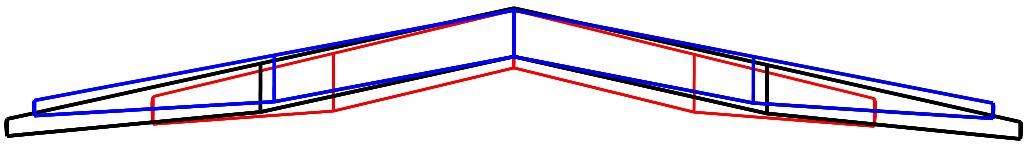

Figure 13. Visualization of the LH2 SBWA wing shapes from the aerostructural optimizations for reference (black), minimum-fuel (blue), and minimum-cost (red) designs.

The inclusion of additional wing design parameters is shown to be beneficial regarding the objective function values. The differences in fuel consumption between the minimum-emission and minimum-cost results are now ca. 4%, compared to 2.5% in SUAVE. Improvements in cost of up to 3.5% are reached, compared to 1.5% in SUAVE. While the changes in wing mass and MTOM are very similar for kerosene and LH2 in SUAVE, the FEMWET results differ. For kerosene, a wing mass reduction of 20% only results in an MTOM reduction of 1.7% when comparing the minimum cost to emission results. For LH2, these changes are larger. A wing weight reduction of 35% is achieved, reducing the MTOM by 5.5%. In this method, the total MTOM is less sensitive to changes in the wing mass.

The improvements in drag are shown in Tables 10 and 11. Both the kerosene and LH2 designs show significant reductions in the overall drag coefficient compared to the reference designs. As the aspect ratios are reducing throughout the optimizations, the induced drag components (CD_i) are larger than the reference. The optimizations of the wing planform, airfoils, and strut result in reduced pressure (wave) and friction drag, shown here as the total parasitic drag of the wing/strut assembly (CD_p).

The minimum-emission results have higher cruise lift coefficients (CL) as the larger structure results in a heavier aircraft throughout the mission.

Table 10. Lift and drag coefficient optimization results for kerosene SBWA.

Parameter	Reference	Min. Emission	Min. Cost
CL	0.3718	0.4237	0.4322
CD	0.0097	0.0072	0.0086
CD_i	0.0019	0.0026	0.0037
CD_p	0.0078	0.0046	0.0049

Table 11. Lift and drag coefficient optimization results for LH2 SBWA.

Parameter	Reference	Min. Emission	Min. Cost
CL	0.3982	0.4155	0.3984
CD	0.0098	0.0065	0.0077
CD_i	0.0022	0.0022	0.0033
CD_p	0.0076	0.0043	0.0044

4. Conclusions

The study investigates the influence of Liquid Hydrogen (LH2) propulsion on the optimal wing geometry of a medium-range Strut-Braced-Wing Aircraft (SBWA) for minimum-

cost and minimum-emission objectives. Multiobjective optimizations are performed in two optimization frameworks of differing fidelity for both kerosene- and LH2-propelled SBWA concepts. A lower-fidelity conceptual-level analysis is used to investigate the Pareto-optimal solutions for both concepts. In a second step, the extremes are analyzed in a higher-fidelity aerostructural optimization to investigate the possibility of further performance gains through more detailed wing-shape optimization.

The results show that the differences in optimal wing geometry between the kerosene- and LH2-powered results for each respective objective function are small. For both aircraft, the minimum-emission objective results optimize towards higher aspect ratios, with the increase in aerodynamic efficiency outweighing the performance penalties due to increased wing structural mass. The minimum-cost objective balances the reductions in fuel and structural masses. A large part of the Direct Operating Cost (DOC) relates to maintenance, capital, and airway costs, which are functions of the Maximum Take-Off Mass (MTOM). The resulting concepts show lower aspect ratios compared to the minimum-emission results, balancing aerodynamic efficiency gains against increases in the wing and strut structural mass due to the higher resulting wing spans. The minimum-cost wings are thicker but have less sweep compared to the minimum-emission wings. Even though the wing aspect ratios for the minimum-cost objectives are ca. 50% higher than for the emission objectives, the actual differences in fuel, emission, and cost are small. Differences in fuel of about 2.5% and differences in DOC of about 1.5% can be expected. While the wing mass for minimum cost is 25% lower, the difference in MTOM is only 4%.

The higher-fidelity results support the discussed trends. Due to a larger set of design variables, including airfoil shapes and strut parameters, further parasite and wave drag reduction opportunities result in increased aspect ratios compared to the conceptual-level optimization results.

The results from both optimization methods show that, for optimal wing shapes of SBWA, the aircraft size and optimization objectives are more relevant than the type of fuel. The benefits in fuel mass for LH2 are balanced with higher structural mass due to dry wings and additional fuel tanks. The differences in the optimal aspect ratio results between the two methods are significant and highlight the necessity to include airfoil shape and strut geometric parameters as further design variables for optimal wing geometry determinations of SBWA.

Future work can focus on increasing the fidelity of the emission models used in the evaluation of the aircraft designs. These models should be sensitive to the actual wing-shape geometries in order to better investigate the effects of wing shape on actual emissions and how to minimize the climate impact of novel airframe concepts.

Author Contributions: Conceptualization, N.F.M.W. and A.E.; methodology, N.F.M.W. and A.E.; software, N.F.M.W. and A.E.; validation, N.F.M.W. and A.E.; writing—original draft preparation, N.F.M.W.; writing—review and editing, N.F.M.W. and A.E.; visualization, N.F.M.W.; supervision, A.E.; project administration, A.E.; funding acquisition, A.E. All authors have read and agreed to the published version of the manuscript.

Funding: This work was supported by the Natural Environment Research Council [NE/Z503824/1].

Data Availability Statement: The data presented in this study is contained within the article.

Conflicts of Interest: The authors declare no conflicts of interest.

Abbreviations

AIC	Aviation-Induced Cloudiness
CF	Correction Factor
DOC	Direct Operating Cost
EI	Emission Index
FEM	Finite Element Method
LH2	Liquid Hydrogen
MDA	Multi-Disciplinary Analysis
MDF	Multi-Disciplinary-Feasible
MTOM	Maximum Take-Off Mass
NLF	Natural Laminar Flow
Q3D	Quasi-Three-Dimensional
SBWA	Strut-Braced-Wing Aircraft
SGTP	Sustained Global Temperature Potential
SLSQP	Sequential Least Squares Quadratic Programming
SUAVE	Stanford University Aerospace Vehicle Environment
T/W	Thrust-to-Weight Ratio
TLR	Top-Level Requirement
UHARW	Ultra-High-Aspect-Ratio Wing
UHBR	Ultra-High-Bypass Ratio
VLM	Vortex Lattice Method
W/S	Wing Loading Ratio
XDSM	Extended Design Structure Matrix

References

1. Advisory Council for Aviation Research and Innovation in Europe. *Realising Europe's Vision for Aviation, Strategic Research & Innovation Agenda*; Technical report; ACARE: Brussels, Belgium, 2012.
2. Greitzer, E.M.; Bonnefoy, P.; De la Rosa Blanco, E.; Dorbian, C.; Drela, M.; Hall, D.; Hansman, R.; Hileman, J.; Liebeck, R.; Lovegren, J.; et al. *N+ 3 Aircraft Concept Designs and Trade Studies, Final Report*; NASA/CR-2010-216794/VOL1; NASA Glenn Research Center: Cleveland, OH, USA, 2010; Volume 44135.
3. Ma, Y.; Elham, A. Designing high aspect ratio wings: A review of concepts and approaches. *Prog. Aerosp. Sci.* **2024**, *145*, 100983. [CrossRef]
4. Karpuk, S.; Elham, A. Conceptual design trade study for an energy-efficient mid-range aircraft with novel technologies. In Proceedings of the AIAA Scitech 2021 Forum, Online, 11–15 and 19–21 January 2021; p. 0013.
5. Hosseini, S.; Ali Vaziri-Zanjani, M.; Reza Ovesy, H. Conceptual design and analysis of an affordable truss-braced wing regional jet aircraft. *Proc. Inst. Mech. Eng. Part G J. Aerosp. Eng.* **2020**, 1–20. [CrossRef]
6. Gur, O.; Schetz, J.A.; Mason, W.H. Aerodynamic considerations in the design of truss-braced-wing aircraft. *J. Aircr.* **2011**, *48*, 919–939. [CrossRef]
7. Shirley, C.M.; Schetz, J.A.; Kapania, R.K.; Haftka, R.T. Tradeoffs of wing weight and lift/drag in design of medium-range transport aircraft. *J. Aircr.* **2014**, *51*, 904–912. [CrossRef]
8. Gundlach IV, J.F.; Tetrault, P.A.; Gern, F.H.; Nagshineh-Pour, A.H.; Ko, A.; Schetz, J.A.; Mason, W.H.; Kapania, R.K.; Mason, W.H.; Grossman, B.; et al. Conceptual design studies of a strut-braced wing transonic transport. *J. Aircr.* **2000**, *37*, 976–983. [CrossRef]
9. Bradley, M.K.; Droney, C.K. *Subsonic Ultra Green Aircraft Research: Phase II—Volume II–Hybrid Electric Design Exploration*; NASA/CR-2015-218704/VOL2; NASA Langley Research Center: Hampton, VA, USA, 2015; p. 378.
10. Torrigiani, F.; Bussemaker, J.; Ciampa, P.D.; Fioriti, M.; Tomasella, F.; Aigner, B.; Rajpal, D.; Timmermans, H.; Savelyev, A.; Charbonnier, D.; et al. Design of the strut braced wing aircraft in the AGILE collaborative MDO framework. In Proceedings of the 31st Congress of the International Council of the Aeronautical Sciences, ICAS, Belo Horizonte, Brazil, 9–14 September 2018.
11. Ma, Y.; Karpuk, S.; Elham, A. Conceptual design and comparative study of strut-braced wing and twin-fuselage aircraft configurations with ultra-high aspect ratio wings. *Aerosp. Sci. Technol.* **2022**, *121*, 107395. [CrossRef]
12. Scholz, D. Calculation of the Emission Characteristics of Aircraft Kerosene and Hydrogen Propulsion. Harvard Data-Verse. 2020. Available online: https://dataverse.harvard.edu/dataset.xhtml?persistentId=doi:10.7910/DVN/DLJUUK (accessed on 20 May 2024).
13. Brewer, G.D. *Hydrogen Aircraft Technology*; CRC Press: Boca Raton, FL, USA, 1991.

14. Karpuk, S.; Elham, A. Comparative study of hydrogen and kerosene commercial aircraft with advanced airframe and propulsion technologies for more sustainable aviation. *Proc. Inst. Mech. Eng. Part G J. Aerosp. Eng.* **2023**, *237*, 2074–2091. [CrossRef]
15. Wahler, N.F.; Ma, Y.; Elham, A. Conceptual Design and Aerostructural Trade-Offs in Hydrogen-Powered Strut-Braced Wing Aircraft: Insights into Dry and Wet Ultra-High Aspect Ratio Wings. *Aerospace* **2025**, *12*, 77. [CrossRef]
16. Chau, T.; Zingg, D.W. Aerodynamic design optimization of a transonic strut-braced-wing regional aircraft. *J. Aircr.* **2022**, *59*, 253–271. [CrossRef]
17. Chakraborty, I.; Nam, T.; Gross, J.R.; Mavris, D.N.; Schetz, J.A.; Kapania, R.K. Comparative assessment of strut-braced and truss-braced wing configurations using multidisciplinary design optimization. *J. Aircr.* **2015**, *52*, 2009–2020. [CrossRef]
18. Gern, F.H.; Ko, A.; Sulaeman, E.; Gundlach, J.F.; Kapania, R.K.; Haftka, R.T. Multidisciplinary design optimization of a transonic commercial transport with strut-braced wing. *J. Aircr.* **2001**, *38*, 1006–1014. [CrossRef]
19. Lukaczyk, T.W.; Wendorff, A.D.; Colonno, M.; Economon, T.D.; Alonso, J.J.; Orra, T.H.; Ilario, C. SUAVE: An open-source environment for multi-fidelity conceptual vehicle design. In Proceedings of the 16th AIAA/ISSMO Multidisciplinary Analysis and Optimization Conference, Dallas, TX, USA, 22–26 June 2015; p. 3087.
20. Karpuk, S.; Ma, Y.; Elham, A. Design Investigation of Potential Long-Range Hydrogen Combustion Blended Wing Body Aircraft with Future Technologies. *Aerospace* **2023**, *10*, 566. [CrossRef]
21. Karpuk, S.; Radespiel, R.; Elham, A. Assessment of future airframe and propulsion technologies on sustainability of next-generation mid-range aircraft. *Aerospace* **2022**, *9*, 279. [CrossRef]
22. Wells, D.P.; Horvath, B.L.; McCullers, L.A. *The Flight Optimization System Weights Estimation Method*; Technical Report NASA/TM-2017-219627/VOL1; NASA Langley Research Center: Hampton, VA, USA, 2017.
23. P. Chiozzotto, G. Initial weight estimate of advanced transport aircraft concepts considering aeroelastic effects. In Proceedings of the 55th AIAA Aerospace Sciences Meeting, Grapevine, TX, USA, 9–13 January 2017; p. 0009.
24. Merkl, E. *Final Report Summary-ENOVAL (Engine Module Validators)*; European Commission: Amsterdam, The Netherlands, 2018.
25. Verstraete, D. The Potential of Liquid Hydrogen for Long Range Aircraft Propulsion. Ph.D. Thesis, Cranfield University, Cranfield, UK, 2009.
26. Lin, C.S.; Van Dresar, N.T.; Hasan, M.M. Pressure control analysis of cryogenic storage systems. *J. Propuls. Power* **2004**, *20*, 480–485. [CrossRef]
27. Elham, A.; van Tooren, M.J. Coupled adjoint aerostructural wing optimization using quasi-three-dimensional aerodynamic analysis. *Struct. Multidiscip. Optim.* **2016**, *54*, 889–906. [CrossRef]
28. Abouhamzeh, M.; Ma, Y.; Elham, A. A Geometrically Nonlinear Structural Model For Aerostructural Optimization of Ultra-High Aspect Ratio Composite Wings. In Proceedings of the AIAA SciTech 2022 Forum, San Diego, CA, USA, 3–7 January 2022; p. 0724.
29. Ma, Y.; Abouhamzeh, M.; Elham, A. Geometrically nonlinear coupled adjoint aerostructural optimization of natural-laminar-flow strut-braced wing. *J. Aircr.* **2023**, *60*, 935–954. [CrossRef]
30. Elham, A.; van Tooren, M. Beyond quasi-analytical methods for preliminary structural sizing and weight estimation of lifting surfaces. In Proceedings of the 56th AIAA/ASCE/AHS/ASC Structures, Structural Dynamics, and Materials Conference, Kissimmee, FL, USA, 5–9 January 2015; p. 0399.
31. Gudmundsson, S. *General Aviation Aircraft Design: Applied Methods and Procedures*; Butterworth-Heinemann: Oxford, UK, 2013.
32. Ma, Y.; Abouhamzeh, M.; Elham, A. Investigating aileron design for ultra-high aspect ratio wings. In Proceedings of the AIAA SCITECH 2023 Forum, National Harbor, MD, USA, 23–27 January 2023; p. 2102.
33. Dillinger, J.; Klimmek, T.; Abdalla, M.M.; Gürdal, Z. Stiffness optimization of composite wings with aeroelastic constraints. *J. Aircr.* **2013**, *50*, 1159–1168. [CrossRef]
34. Roskam, J. *Airplane Design, Part i: Preliminary Sizing of Airplanes, Design*; Analysis and Research Corporation: Lawrence, KS, USA, 1997.
35. Boozer, C.M.; Elham, A. Coupled Adjoint Aerostructural Optimization Framework for Preliminary Aircraft Design. In Proceedings of the 31st Congress of the International Council of the Aeronautical Sciences, Belo Horizonte, Brazil, 9–14 September 2018.
36. Elham, A.; van Tooren, M.J. Tool for preliminary structural sizing, weight estimation, and aeroelastic optimization of lifting surfaces. *Proc. Inst. Mech. Eng. Part G J. Aerosp. Eng.* **2016**, *230*, 280–295. [CrossRef]
37. Bardenhagen, A.; Gobbin, A. *Flugzeugentwurf II*; Universität Stuttgart: Stuttgart, Germany, 2017.
38. Roskam, J. *Airplane Design Part I–VIII*; Roskam Aviation and Engineering Corp.: Ottawa, KS, USA, 1985.
39. Hoelzen, J.; Silberhorn, D.; Zill, T.; Bensmann, B.; Hanke-Rauschenbach, R. Hydrogen-powered aviation and its reliance on green hydrogen infrastructure–Review and research gaps. *Int. J. Hydrogen Energy* **2022**, *47*, 3108–3130. [CrossRef]
40. Scholz, D. Design of hydrogen passenger aircraft: How much "zero-emission" is possible? In Proceedings of the Hamburg Aerospace Lecture Series, Hamburg, Germany, 19 November 2020.
41. Baughcum, S.L.; Tritz, T.G.; Henderson, S.C.; Pickett, D.C. *Scheduled Civil Aircraft Emission Inventories for 1992: Database Development and Analysis*; Technical Report NASA-CR-4700; NASA Langley Research Center: Hampton, VA, USA, 1996.
42. Dallara, E.S. Aircraft Design for Reduced Climate Impact. Ph.D. Thesis, Stanford University, Stanford, CA, USA, 2011.

43. Howarth, R.W.; Jacobson, M.Z. How green is blue hydrogen? *Energy Sci. Eng.* **2021**, *9*, 1676–1687. [CrossRef]
44. Engesser, F. *Die Knickfestigkeit Gerader Stäbe*; W. Ernst & Sohn: Berlin, Germany, 1891.
45. EASA. *CS-25 Large Aeroplanes, Amendment 28*; Technical Report; European Union Aviation Safety Agency: Cologne, Germany, 2023.
46. Ma, Y.; Minisci, E.; Elham, A. Investigating the influence of uncertainty in novel airframe technologies on realizing ultra-high aspect ratio wings. In Proceedings of the AeroBest 2021, Lisboa, Portugal, 21–23 July 2021.
47. Airbus SAS. A320-Aircraft Characteristics Airport and Maintenance Planning. 2024. Available online: https://aircraft.airbus.com/sites/g/files/jlcbta126/files/2025-01/AC_A320_0624.pdf (accessed on 20 May 2024).